J|A|C|S
ARTICLES
Published on Web 01/29/2004

NMR $R_{1\rho}$ Rotating-Frame Relaxation with Weak Radio Frequency Fields

Francesca Massi,[†] Eric Johnson,[‡] Chunyu Wang,[†] Mark Rance,*[,‡] and Arthur G. Palmer, III*[,†]

Contribution from the Department of Biochemistry and Molecular Biophysics, Columbia University, 630 West 168th Street, New York, New York 10032, and Department of Molecular Genetics, Biochemistry, and Microbiology, University of Cincinnati College of Medicine, 231 Albert Sabin Way, Cincinnati, OH 45267-0524

Received September 25, 2003; E-mail: rance@rabi.med.uc.edu; agp6@columbia.edu

Abstract: NMR spin relaxation in the rotating frame ($R_{1\rho}$) is one of few methods available to characterize chemical exchange kinetic processes occurring on μs−ms time scales. $R_{1\rho}$ measurements for heteronuclei in biological macromolecules generally require decoupling of ^{1}H scalar coupling interactions and suppression of cross-relaxation processes. Korzhnev and co-workers demonstrated that applying conventional ^{1}H decoupling schemes while the heteronuclei are spin-locked by a radio frequency (rf) field results in imperfect decoupling [Korzhnev, Skrynnikov, Millet, Torchia, Kay. *J. Am. Chem. Soc.* **2002**, *124*, 10743−10753]. Experimental NMR pulse sequences were presented that provide accurate measurements of $R_{1\rho}$ rate constants for radio frequency field strengths > 1000 Hz. This paper presents new two-dimensional NMR experiments that allow the use of weak rf fields, between 150 and 1000 Hz, in $R_{1\rho}$ experiments. Fourier decomposition and average Hamiltonian theory are employed to analyze the spin-lock sequence and provide a guide for the development of improved experiments. The new pulse sequences are validated using ubiquitin and basic pancreatic trypsin inhibitor (BPTI). The use of weak spin-lock fields in $R_{1\rho}$ experiments allows the study of the chemical exchange process on a wider range of time scales, bridging the gap that currently exists between Carr−Purcell−Meiboom−Gill and conventional $R_{1\rho}$ experiments. The new experiments also extend the capability of the $R_{1\rho}$ technique to study exchange processes outside the fast exchange limit.

1. Introduction

Biological functions of proteins, such as catalysis and ligand binding, necessarily are associated with chemical transformations and conformational transitions.[1] Nuclear magnetic resonance (NMR) spectroscopy is sensitive to dynamic processes in proteins with atomic resolution on a wide range of time scales. Dynamic processes on μs−ms time scales increase the relaxation rate constants for transverse magnetization because chemical or conformational changes that alter local magnetic environments introduce a stochastic time dependence of the resonance frequencies of the affected nuclear spins. Such dynamic phenomena in NMR spectroscopy are referred to as chemical exchange processes. The Carr−Purcell−Meiboom−Gill (CPMG) and $R_{1\rho}$ spin relaxation experiments are two major techniques for measuring transverse relaxation rate constants and characterizing chemical exchange processes on μs−ms time scales.[2] Several studies have proven the usefulness of CPMG[3−7] and $R_{1\rho}$[8−11] techniques for achieving detailed insights into kinetic processes in biological systems.

$R_{1\rho}$ rotating-frame relaxation experiments lock magnetization along the direction of the effective field in the rotating frame by application of a radio frequency (rf) field. The experiment can be performed using near-resonance or off-resonance rf fields, respectively, called on-resonance and off-resonance $R_{1\rho}$ experiments. The relaxation rate constant, $R_{1\rho}$, for decay of the magnetization component parallel to the effective field in the rotating frame, ω_e, is a function of the amplitude of the applied rf field, ω_1, and of the resonance offset from the spin-lock carrier, Ω. Parameters that characterize the kinetics of the chemical exchange process are obtained from the variation of $R_{1\rho}$ as a function of ω_e, called relaxation dispersion.[2] CPMG relaxation experiments monitor the decay of transverse magnetization in a series of spin−echo pulse sequence elements. Chemical exchange is characterized from the variation in the

[†] Columbia University.
[‡] University of Cincinnati College of Medicine.

(1) Fersht, A. *Structure and mechanism in protein science: a guide to enzyme catalysis and protein folding*; W. H. Freeman: New York, 1999.
(2) Palmer, A. G.; Kroenke, C. D.; Loria, J. P. *Methods Enzymol.* **2001**, *339*, 204−238.
(3) Grey, M. J.; Wang, C.; Palmer, A. G. *J. Am. Chem. Soc.* **2003**, *125*, 14324−14335.
(4) Mulder, F. A. A.; Mittermaier, A.; Hon, B.; Dahlquist, F. W.; Kay, L. E. *Nat. Struct. Biol.* **2001**, *8*, 932−935.
(5) Kovrigin, E. L.; Cole, R.; Loria, J. P. *Biochemistry* **2003**, *42*, 5279−5291.
(6) Ishima, R.; Freedberg, D. I.; Wang, Y. X.; Louis, J. M.; Torchia, D. A. *Structure* **1999**, *7*, 1047−1055.
(7) Eisenmesser, E. Z.; Bosco, D. A.; Akke, M.; Kern, D. *Science* **2002**, *295*, 1520−1523.
(8) Akke, M.; Palmer, A. G. *J. Am. Chem. Soc.* **1996**, *118*, 911−912.
(9) Akke, M.; Liu, J.; Cavanagh, J.; Erickson, H. P.; Palmer, A. G. *Nat. Struct. Biol.* **1998**, *5*, 55−59.
(10) Mulder, F. A. A.; van Tilborg, P. J. A.; Kaptein, R.; Boelens, R. *J. Biomol. NMR* **1999**, *13*, 275−288.
(11) Vugmeyster, L.; Kroenke, C. D.; Picard, F.; Palmer, A. G.; Raleigh, D. P. *J. Am. Chem. Soc.* **1996**, *122*, 5387−5388.

transverse relaxation rate constant, R_2, as a function of the time delay between refocusing pulses in the spin−echo sequence, τ_{cp}. An effective field strength for the CPMG experiment can be defined as $\omega_{CPMG} = 12^{1/2}/\tau_{cp}$ to illustrate the fundamental similarity of these two methods.[12]

Line shape analysis also is widely used to study exchange processes;[13,14] however, more detailed investigation is possible by $R_{1\rho}$ and CPMG experiments because the rf field strength and pulsing rate provide additional variables under experimental control.

^{13}C and ^{15}N $R_{1\rho}$ relaxation experiments in biological macromolecules typically use effective rf field strengths, $\nu_e = \omega_e/(2\pi)$, of the order of 1−6 kHz to ensure that $\nu_e \gg J$, where J is the $^1H-^{13}C$ or $^1H-^{15}N$ scalar coupling constant. CPMG relaxation experiments typically use effective field strengths, $\nu_{CPMG} = \omega_{CPMG}/(2\pi)$, on the order of 25−500 Hz corresponding to τ_{cp} 22−1 ms, being limited by the maximum pulsing rate that is experimentally feasible. As a result, CPMG experiments are used most often to measure slower, ms timescale, and $R_{1\rho}$ are used most often to characterize faster, μs timescale, chemical exchange processes.

Recent theoretical[15−17] and experimental[18] studies have demonstrated that $R_{1\rho}$ rotating frame experiments have unique advantages in the characterization of exchange processes outside the fast exchange limit. In particular, when exchange results from transitions between chemical states with site populations that are highly skewed, the $R_{1\rho}$ experiment becomes sensitive to the resonance frequency of the minor species, rather than the dominant species. As a result, complete characterization of an exchange process is possible using relaxation data acquired at a single static magnetic field strength by varying both the field strength and resonance frequency of the rf field. In contrast, the CPMG experiment normally requires that data be acquired at multiple static magnetic field strengths.[19]

This paper describes $R_{1\rho}$ experiments that utilize weak rf fields ranging from 150 to 1000 Hz. These experiments bridge the time scale gap between the CPMG and conventional $R_{1\rho}$ experiments using strong rf fields >1000 Hz and facilitate the use of $R_{1\rho}$ methods for characterizing slow exchange processes. The new pulse sequences extend the applicability of $R_{1\rho}$ relaxation dispersion to the study of a broader range of exchange processes in biological macromolecules.

The major difficulty in the use of weak rf fields in ^{13}C or ^{15}N $R_{1\rho}$ experiments arises because ^1H 180° pulses or ^1H decoupling sequences must be used to suppress the effects of cross-correlation between dipole−dipole (DD) and chemical shift anisotropy (CSA) relaxation mechanisms.[20−22] As shown by Korzhnev and co-workers, the methods used to suppress cross correlation can result in incomplete decoupling of the scalar coupling interaction and lead to overestimation of $R_{1\rho}$ rate constants.[23] The errors in the $R_{1\rho}$ rate constants become more severe as spin-lock field strength decreases. This article presents a theoretical analysis of the $R_{1\rho}$ experiment that guided the design of modified pulse sequences capable of using lower spin lock field strengths. The new pulse sequences were validated using ubiquitin and basic pancreatic trypsin inhibitor (BPTI).

The remainder of the paper is organized as follows: (i) The experimental methods used to validate the new pulse sequences are described. (ii) The theoretical analysis used to develop the new pulse sequences is outlined. (iii) Experimental results for ^{15}N $R_{1\rho}$ relaxation in ubiquitin and BPTI are presented. (iv) The theoretical and experimental results are discussed.

2. Materials and Methods

NMR ^{15}N relaxation measurements were performed on 1.25 mM [$U-^{15}N$] sample of ubiquitin (90% H_2O/10% D_2O, 10 mM sodium phosphate buffer, pH 5.8, $T = 298$ K) and on a 1.4 mM [$U-^{15}N$] sample of BPTI (90% H_2O/10% D_2O, pH 5.1, $T = 300$ K). Ubiquitin relaxation data were collected at a static magnetic field strength of 11.7 T, using a Bruker DRX500 or Varian Inova 500 NMR spectrometer. BPTI data were collected at 14.1 T, using a Bruker DRX600 spectrometer. Temperatures were calibrated using a sample of 100% methanol. Relaxation rate constants were determined from a series of two-dimensional spectra recorded with different relaxation delays (11 or 12 spectra, including duplicates). Intensities of cross-peaks were fitted to monoexponential decay functions to give ^{15}N spin relaxation rate constants; uncertainties were estimated by jackknife simulations.[24] Spectra were processed using nmrPipe,[25] Sparky,[26] and Curvefit (www.palmer.hs.columbia.edu).

^{15}N R_1 and R_2 values were measured as described previously using inversion recovery and CPMG experiments.[27] Maximum relaxation delay values of 800 ms and 200 ms were used for R_1 and R_2, respectively. The interval between ^{15}N 180° pulses in the CPMG sequence of the R_2 experiment was equal to 1 ms.

^{15}N $R_{1\rho}$ rate constants were measured using the pulse sequences shown in Figure 1.[8,23] The pulse sequences consist of a refocused INEPT polarization transfer scheme,[28,29] a spin-lock relaxation period of total length τ, the indirect t_1 labeling period, and a gradient PEP sensitivity enhanced detection scheme.[30,31] Before and after each spin-lock period, ^{15}N magnetization was rotated between the z-axis of the rotating reference frame and the z-axis of the tilted reference frame using the pulse sequence element $90^\circ_\phi - \chi - 90^\circ_{\phi-\pi/2}$, where $\phi = x$ or y, $\chi = 1/\omega_1 - 4\tau_{90}/\pi$, ω_1 is the Rabi amplitude of the radio frequency spin-lock field, and τ_{90} is the length of the 90° pulses.[32] This method relies on the approximation that $\tan\beta \approx \beta$, where $\beta = \Omega/\nu_1$. This approximation is valid when $|\beta|$ is small. Therefore only resonances with $|\beta| \leq 0.4$ were analyzed, corresponding to an alignment error of ≤5%. Three different schemes were employed to suppress scalar coupling evolution and $^1H-^{15}N$ DD/^{15}N CSA relaxation interference.

(12) Ishima, R.; Torchia, D. A. *J. Biomol. NMR* **1999**, *14*, 369−372.
(13) Rao, B. D. N. *Methods Enzymol.* **1989**, *176*, 279−311.
(14) Lian, L. Y.; Barsukov, I. L.; Sutcliffe, M. J.; Sze, K. H.; Roberts, G. C. K. *Methods Enzymol.* **1994**, *239*, 657−700.
(15) Trott, O.; Palmer, A. G. *J. Magn. Reson.* **2002**, *154*, 157−160.
(16) Trott, O.; Abergel, D.; Palmer, A. G. *Mol. Phys.* **2003**, *101*, 753−763.
(17) Abergel, D.; Palmer, A. G. *Concepts Magn. Reson.* **2003**, *19A*, 134−148.
(18) Korzhnev, D. M.; Orekhov, V. Y.; Dahlquist, F. W.; Kay, L. E. *J. Biomol. NMR* **2003**, *26*, 39−48.
(19) Millet, O.; Loria, J. P.; Kroenke, C. D.; Pons, M.; Palmer, A. G. *J. Am. Chem. Soc.* **2000**, *122*, 2867−2877.
(20) Boyd, J.; Hommel, U.; Campbell, I. D. *Chem. Phys. Lett.* **1990**, *175*, 477−482.
(21) Palmer, A. G.; Skelton, N. J.; Chazin, W. J.; Wright, P. E.; Rance, M. *Mol. Phys.* **1992**, *75*, 699−711.
(22) Kay, L. E.; Nicholson, L. K.; Delaglio, F.; Bax, A.; Torchia, D. A. *J. Magn. Reson.* **1992**, *97*, 359−375.
(23) Korzhnev, D. M.; Skrynnikov, N. S.; Millet, O.; Torchia, D. A.; Kay, L. E. *J. Am. Chem. Soc.* **2002**, *124*, 10743−10753.
(24) Philippopoulos, M.; Lim, C. *J. Mol. Biol.* **1995**, *254*, 771−792.
(25) Delaglio, F.; Grzesiek, S.; Vuister, G. W.; Zhu, G.; Pfeifer, J.; Bax, A. *J. Biomol. NMR* **1995**, *6*, 277−293.
(26) Goddard, T. D.; Kneller, D. G. *SPARKY 3*; University of California, San Francisco.
(27) Farrow, N. A.; Muhandiram, R.; Singer, A. U.; Pascal, S. M.; Kay, C. M.; Gish, G.; Shoelson, S. E.; Pawson, T.; Forman-Kay, J. D.; Kay, L. E. *Biochemistry* **1994**, *33*, 5984−6003.
(28) Morris, G. A.; Freeman, R. *J. Am. Chem. Soc.* **1979**, *101*, 760−762.
(29) Burum, D. P.; Ernst, R. R. *J. Magn. Reson.* **1980**, *39*, 163−168.
(30) Palmer, A. G.; Cavanagh, J.; Wright, P. E.; Rance, M. *J. Magn. Reson.* **1991**, *93*, 151−170.
(31) Kay, L. E.; Keifer, P.; Saarinen, T. *J. Am. Chem. Soc.* **1992**, *114*, 10663−10665.
(32) Yamazaki, T.; Muhandiram, R.; Kay, L. E. *J. Am. Chem. Soc.* **1994**, *116*, 8266−8278.

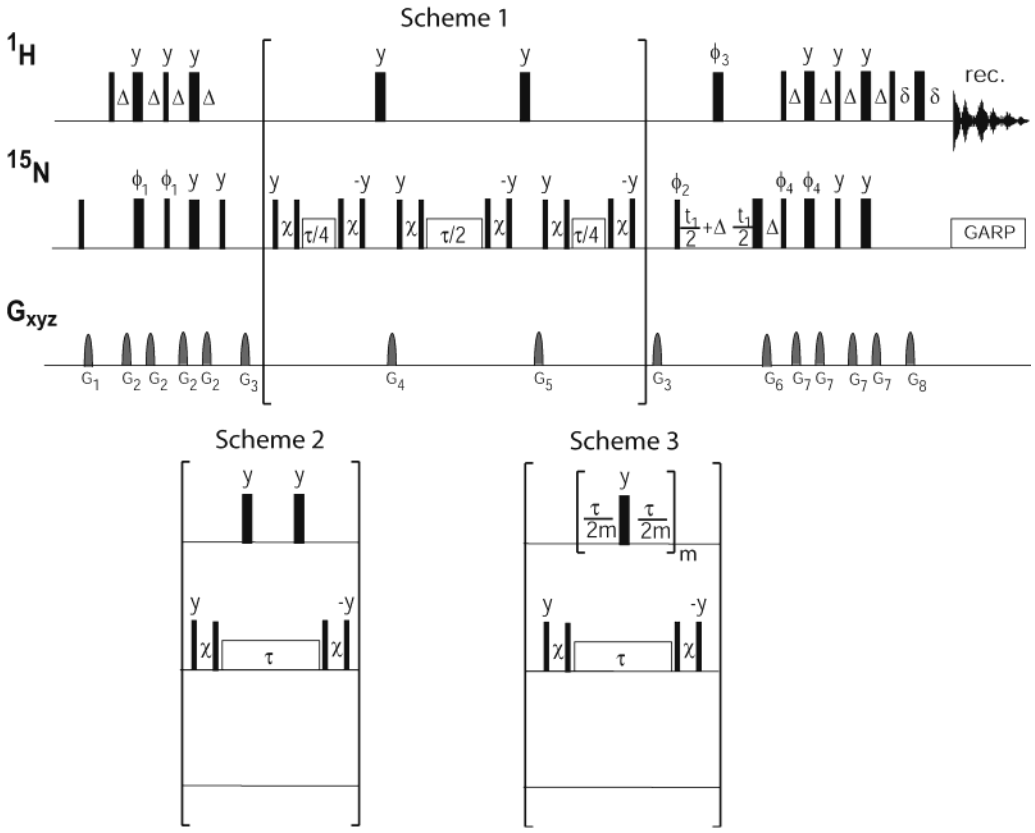

Figure 1. Pulse sequences for the measurement of ^{15}N $R_{1\rho}$. Narrow and wide filled bars indicate 90° and 180° pulses, respectively. All pulses are applied with phase x unless otherwise indicated. Open rectangles indicate spin-lock periods, always applied with phase x. All ^{1}H pulses are applied with the carrier frequency centered on the water resonance with the exception of those applied during the periods described in Schemes 1, 2, and 3 which are applied in the center of the amide region. Delays are $\Delta = 2.7$ ms, $\chi = 1/\omega_1 - 4\tau_{90}/\pi$, where ω_1 is the spin-lock field strength, and $\delta = 0.406$ ms. The total length of the spin-lock period is equal to τ. ^{15}N decoupling during acquisition is performed using a 1.25 kHz GARP sequence.[44] The phase cycle is $\phi_1 = x - x$; $\phi_2 = 2(x)$, $2(-x)$; $\phi_3 = 4(x)$, $4(-x)$; $\phi_{rec} = x, -x, -x, x$. The gradients are sine shaped of length (in ms) equal to $G_1 = 2.0$, $G_2 = 0.2$, $G_3 = 1.5$, $G_4 = 1.0$, $G_5 = 1.0$, $G_6 = 2.0$, $G_7 = 0.4$, and $G_8 = 0.2$ and of strength (in G/cm) equal to $G_{1z} = 9$, $G_{2z} = 4$, $G_{3z} = 10$, $G_{4xyz} = 25$, $G_{5xyz} = 20$, $G_{6xyz} = 40$, $G_{7z} = 5$, $G_{8xyz} = 40$. G_6 and G_8 are used for gradient coherence selection. Gradient PEP coherence selection is obtained by inverting the sign of gradient G_6 and phase ϕ_4.[31] In Scheme 3, a different number of ^{1}H 180° pulses, m, is applied depending on the length of the spin-lock period, τ, with $0 \le \tau \le \tau_{max}$.[23] For $0 \le \tau < \tau_{max}/3$, $m = 0$ and no ^{1}H 180° pulses are applied. For $\tau_{max}/3 \le \tau < 2\tau_{max}/3$, $m = 1$; for $2\tau_{max}/3 \le \tau < \tau_{max}$, $m = 2$; and for $\tau = \tau_{max}$, $m = 3$.

Scheme 3 was recently proposed and validated by Korzhnev and coworkers for field strengths $\omega_1 > 1000$ Hz.[23] In this approach, the number of 180° ^{1}H decoupling pulses applied depends on the length of τ as described in the figure caption. Scheme 2 uses two 180° ^{1}H pulses applied at $\tau/4$ and $3\tau/4$ during the spin-lock period. Scheme 1 effectively uses two 180° ^{1}H pulses applied at $\tau/4$ and $3\tau/4$, but ^{15}N magnetization is returned to the z-axis and the rf field turned off prior to the pulses; after the 180° ^{1}H pulses, field gradient pulses are applied to dephase any transverse magnetization components.

The performance of each of the decoupling schemes in Figure 1 was evaluated by measuring $R_{1\rho}$ using the ubiquitin sample. $R_{1\rho}$ experiments were performed at four different spin-lock field strengths (1000, 500, 250, and 150 Hz). The maximum length of the spin-lock period in all the experiments was equal to 160 ms.

Relaxation dispersion was measured for the backbone ^{15}N amide spin in residue Cys 14 in BPTI. This resonance is known to undergo chemical exchange broadening due to isomerization of the Cys 14−Cys 38 disulfide bond.[3] $R_{1\rho}$ experiments described in the pulse sequence depicted in Scheme 1 of Figure 1 were performed on the BPTI sample using 10 different spin-lock field strengths (178 ± 6, 277 ± 3, 424 ± 3, 542 ± 3, 689 ± 4, 806 ± 3, 904 ± 3, 1000 ± 3, 1099 ± 3, 1235 ± 3 Hz). In addition, off-resonance $R_{1\rho}$ experiments, where the spin-lock rf frequency was set outside the spectral region of interest, were performed using a spin-lock field strength of 1220 ± 4 Hz and resonance offsets of 1213 and 1734 Hz. These experiments were performed using the pulse sequence of Scheme 2 of Figure 1 except that the $90^\circ_\phi - \chi - 90^\circ_{\phi-\pi/2}$ elements were replaced by tanh/tan adiabatic sweeps.[33] The tanh/tan adiabatic pulse had a duration of 10 ms, and the frequency sweep began at −15 000 Hz from the carrier frequency. The maximum length of the spin-lock period in all the experiments was equal to 120 ms.

The relaxation rate constant in the rotating frame is given by[34,35]

$$R_{1\rho} = R_1 \cos^2\theta + R_2 \sin^2\theta \qquad (1)$$

where $\theta = \arctan(\omega_1/\Omega)$ and Ω is the resonance offset from the spin-lock carrier frequency. Thus, ^{15}N R_2 rate constants can be calculated using measured values of $R_{1\rho}$ and R_1 relaxation rate constants. Standard methods for error propagation have been used to estimate the uncertainties in R_2 arising from experimental uncertainties in $R_{1\rho}$, R_1, and θ. In the presence of an exchange process, $R_2 = R_2^0 + R_{ex}$, in which R_2^0 is the relaxation rate constant due to relaxation mechanisms other than exchange. For two-site exchange that is fast on the chemical shift time scale,[2]

$$R_{ex} = k_{ex}\Phi_{ex}/(k_{ex}^2 + \omega_e^2) \qquad (2)$$

(33) Mulder, F. A. A.; de Graaf, R. A.; Kaptein, R.; Boelens, R. *J. Magn. Reson.* **1998**, *131*, 351−357.
(34) Abragam, A. *Principles of nuclear magnetism;* Oxford University Press: Oxford, 1983.
(35) Deverell, C.; Morgan, R. E.; Strange, J. H. *Mol. Phys.* **1970**, *18*, 553−559.

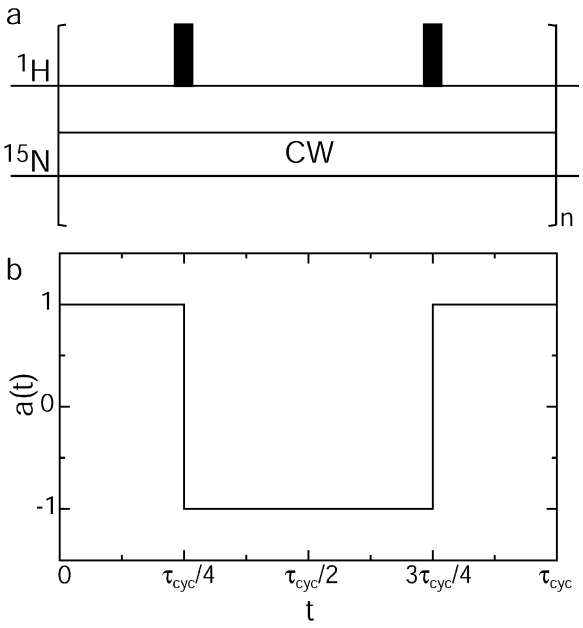

Figure 2. ^{1}H decoupling during ^{15}N spin-locking sequences. (a) Decoupling is achieved for a total spin-lock period $\tau = n\tau_{cyc}$ by applying ^{1}H 180° pulses at $\tau_{cyc}/4$ and $3\tau_{cyc}/4$. (b) $a(t)$ describes the sign of the scalar coupling Hamiltonian in eq 3 as a function of time; every time an ^{1}H 180° pulse is applied, $a(t)$ changes sign.

where k_{ex} is the exchange rate constant, $\Phi_{ex} = p_A p_B \delta\omega^2$, p_A and p_B are the fractional populations of sites A and B, and $\delta\omega$ is the difference between the ^{15}N chemical shifts of the two sites A and B.

The spin-lock field strengths used in the $R_{1\rho}$ experiments were calibrated by off-resonance continuous wave decoupling as previously described.[2] Reported uncertainties are obtained from curvefitting. Variation in ω_1 due to B_1 inhomogeneity is ~10% as measured by a transient nutation experiment.[36]

3. Theory

We begin by analyzing the spin-lock sequence shown in Figure 2a. In this scheme, 180° ^{1}H decoupling pulses are applied at $\tau_{cyc}/4$ and $3\tau_{cyc}/4$, and the scheme is repeated cyclically such that $\tau = n\tau_{cyc}$. This decoupling scheme has been analyzed by Korzhnev and co-workers using a local field approach.[23] Herein, we use a Fourier decomposition and average Hamiltonian theory[37] to provide additional insight and guide the development of improved pulse sequences.

The effective S spin Hamiltonian in the rotating reference frame during the period τ can be written as[38]

$$H(t) = \Omega S_z + \omega_1 S_x + a(t)2\pi J I_z S_z \tag{3}$$

where $a(t)$ is the periodic square wave function shown in Figure 2b, the radio frequency field is assumed to have x-phase, and J is the $I-S$ scalar coupling constant. Operators I and S refer to ^{1}H and ^{15}N, respectively. In this picture, the effect of the ^{1}H 180° pulses is to introduce a time dependence into the scalar coupling Hamiltonian. The Fourier series of $a(t)$ is

$$a(t) = \sum_{k=0}^{\infty} \frac{(-1)^k 4}{(2k+1)\pi} \cos(2\pi(2k+1)t/\tau_{cyc}) \tag{4}$$

To analyze the effect of the scalar coupling interaction on the $R_{1\rho}$ relaxation experiment, we change to a tilted reference frame defined by a unitary transformation $\hat{H}(t) = U_1 H(t) U_1^{-1}$ with $U_1 = \exp[i\theta S_y]$. The z-axis of the tilted frame is oriented at an angle θ relative to z-axis of the rotating frame. In the tilted frame, the Hamiltonian becomes

$$\hat{H}(t) = \omega_e S'_z + a(t)2\pi J(I_z S'_z \cos\theta - I_z S'_x \sin\theta) \tag{5}$$

in which $\omega_e = (\Omega^2 + \omega_1^2)^{1/2}$. The propagator for evolution under $\hat{H}(t)$ is given by

$$U(t) = T\exp\{-i\int_0^t \hat{H}(t')\,dt'\} \tag{6}$$

in which T is the Dyson time-ordering operator.[39] This propagator can be written as:[37]

$$U(t) = U_0(t)U_J(t) \tag{7}$$

where

$$U_0(t) = \exp\{-i\omega_e S'_z t\} \tag{8}$$

$$U_J(t) = T\exp\{-i\int_0^t \tilde{H}(t')\,dt'\} = \exp\{-i\bar{H}t\} \tag{9}$$

$\tilde{H}$ is the effective Hamiltonian in an interaction frame rotating around S'_z with frequency ω_e:

$$\tilde{H} = a(t)2\pi J U_2(I_z S'_z \cos\theta - I_z S'_x \sin\theta)U_2^{-1} \tag{10}$$

$$= a(t)2\pi J I_z S'_z \cos\theta - a(t)2\pi J I_z S'_x \sin\theta \cos\omega_e t + a(t)2\pi J I_z S'_y \sin\theta \sin\omega_e t$$

in which $U_2 = \exp[i\omega_e t S'_z]$. $\bar{H}$ is the average Hamiltonian given by[39]

$$\bar{H} = \bar{H}^{(0)} + \bar{H}^{(1)} + \ldots \tag{11}$$

in which

$$\bar{H}^{(0)} = \frac{1}{t}\int_0^t \tilde{H}(t_1)\,dt_1 \tag{12}$$

$$\bar{H}^{(1)} = \frac{-i}{2t}\int_0^t dt_2 \int_0^{t_2} [\tilde{H}(t_2), \tilde{H}(t_1)]\,dt_1 \tag{13}$$

are the zeroth- and first-order contributions to the average Hamiltonian. In general, $\bar{H}$, $\bar{H}^{(0)}$, and $\bar{H}^{(1)}$ are functions of t. However, if $\omega_e\tau_{cyc} = 2m\pi$, where m is an integer, then $U_0(\tau_{cyc}) = 1$,

$$U(n\tau_{cyc}) = U_J^n(\tau_{cyc}) \tag{14}$$

and the average Hamiltonian is defined for $t = \tau_{cyc}$ in eq 12.

The average Hamiltonian is calculated by expanding the trigonometric functions in eq 10 and integrating term by term. The first term in eq 10 does not contribute to $\bar{H}^{(0)}$ because the

(36) Guenneugues, M.; Berthault, P.; Desvaux, H. *J. Magn. Reson.* **1999**, *136*, 118−126.
(37) Haeberlen, U.; Waugh, J. S. *Phys. Rev.* **1968**, *175*, 453−467.
(38) Jaroniec, C. P.; Tounge, B. A.; Rienstra, C. M.; Herzfeld, J.; Griffin, R. G. *J. Magn. Reson.* **2000**, *146*, 132−139.
(39) Ernst, R. R.; Bodenhausen, G.; Wokaun, A. *Principles of nuclear magnetic resonance in one and two dimensions*; Oxford University Press: Oxford, 1987.

average value of $a(t)$ is zero. Using $a(t)$ given in eq 4, the second and third terms of eq 10 are expanded as

$$\begin{aligned} &- a(t)\, 2\pi J I_z S'_x \sin\theta \cos\omega_e t + a(t) 2\pi J I_z S'_y \sin\theta \sin\omega_e t \\ &= -2\pi J \sin\theta\, I_z S'_x \sum_{k=0}^{\infty} \frac{(-1)^k 2}{(2k+1)\pi} \{\cos[2\pi(2k+1)/\tau_{cyc} + \omega_e]t \\ &\quad + \cos[2\pi(2k+1)/\tau_{cyc} - \omega_e]t\} + \\ &\quad 2\pi J \sin\theta I_z S'_y \sum_{k=0}^{\infty} \frac{(-1)^k 2}{(2k+1)\pi} \{\sin[2\pi(2k+1)/\tau_{cyc} + \omega_e]t \\ &\quad - \sin[2\pi(2k+1)/\tau_{cyc} - \omega_e]t\} \end{aligned} \tag{15}$$

The contributions of the first and third terms of eq 15 to $\bar{H}^{(0)}$ approach zero rapidly when $[2\pi(2k+1)/\tau_{cyc} + \omega_e]t \gg 1$ and can be neglected (vide infra). Keeping only the second and fourth terms, the parts of $\tilde{H}(t)$ that contribute significantly to $\bar{H}^{(0)}$ are

$$\begin{aligned} \tilde{H}(t) \approx 2\pi\, J \sin\theta \sum_{k=0}^{\infty} \frac{(-1)^{k+1} 2}{(2k+1)\pi} \\ \times \{\cos[(2k+1-\nu_e\tau_{cyc})2\pi t/\tau_{cyc}] I_z S'_x \\ + \sin[(2k+1-\nu_e\tau_{cyc})2\pi t/\tau_{cyc}] I_z S'_y\} \end{aligned} \tag{16}$$

Whenever $\nu_e\tau_{cyc}$ is an integer, the propagator is given by eq 14. In this situation, $\tilde{H}(t)$ and, consequently, $\bar{H}^{(0)}$ vanish unless the condition

$$\nu_e\tau_{cyc} = 2k+1 \tag{17}$$

is also satisfied. In this special case, $\bar{H}^{(0)}$ is obtained simply as

$$\bar{H}^{(0)} = 2\pi\, \bar{J} I_z S'_x \tag{18}$$

with

$$\bar{J} = (-1)^{(\nu_e\tau_{cyc}+1)/2} \frac{2J\sin\theta}{\pi\nu_e\tau_{cyc}} \tag{19}$$

Equations 17 and 19 are equivalent to eqs 5.1 and 6 of Korzhnev et al., respectively.[23] Thus, the local field approach of Korzhnev and co-workers is equivalent to average Hamiltonian theory under the condition that $U_0(\tau_{cyc})$ is cyclic.

More generally, the lowest order contribution to the average Hamiltonian calculated over the full spin lock period, $\tau = n\tau_{cyc}$, is given by

$$\begin{aligned} \bar{H}^{(0)} = 2I_z S'_x \frac{2J\sin\theta}{2\pi n} \sum_{k=0}^{\infty} \frac{(-1)^k \sin(2\pi n\nu_e\tau_{cyc})}{(2k+1)[(2k+1)-\nu_e\tau_{cyc}]} + \\ 2I_z S'_y \frac{2J\sin\theta}{2\pi n} \sum_{k=0}^{\infty} \frac{(-1)^k [\cos(2\pi n\nu_e\tau_{cyc}) - 1]}{(2k+1)[(2k+1)-\nu_e\tau_{cyc}]} \end{aligned} \tag{20}$$

This expression can be simplified by switching to a new reference frame obtained by a rotation around S'_z by an angle:

$$\begin{aligned} \phi &= \arctan\left[\frac{\cos(2\pi n\nu_e\tau_{cyc}) - 1}{\sin(2\pi n\nu_e\tau_{cyc})}\right] \\ &= -\pi n\nu_e\tau_{cyc} \end{aligned} \tag{21}$$

In the new frame,

$$\bar{H}^{(0)} = 2\pi\, \bar{J} I_z S''_x \tag{22}$$

where

$$\begin{aligned} \bar{J} &= \frac{2J\sin\theta}{n\pi^2} \sin(n\pi\nu_e\tau_{cyc}) \sum_{k=0}^{\infty} \frac{(-1)^k}{(2k+1)[(2k+1)-\nu_e\tau_{cyc}]} \\ &= \frac{J\sin\theta}{2n\pi^2\nu_e\tau_{cyc}} \sin(n\pi\nu_e\tau_{cyc}) \\ &\quad \times \left[-\pi - \psi\left(\frac{1-\nu_e\tau_{cyc}}{4}\right) + \psi\left(\frac{3-\nu_e\tau_{cyc}}{4}\right)\right] \end{aligned} \tag{23}$$

where $\psi(x)$ is the digamma function.[40]

The evolution of the $S'_z = S''_z$ magnetization is thus

$$\begin{aligned} S'_z(\tau = n\tau_{cyc}) &= S'_z(0)\cos(\pi\, \bar{J} n\tau_{cyc}) \exp(-R_{1\rho} n\tau_{cyc}) \\ &= S'_z(0)\cos[n(J/\nu_e)\sin\theta F_n(\nu_e\tau_{cyc})] \exp(-R_{1\rho} n\tau_{cyc}) \end{aligned} \tag{24}$$

where exponential decay of the spin-locked magnetization has been assumed and

$$\begin{aligned} F_n(\nu_e\tau_{cyc}) = \frac{\sin(n\pi\nu_e\tau_{cyc})}{2n\pi} \left[-\pi - \psi\left(\frac{1-\nu_e\tau_{cyc}}{4}\right) + \right. \\ \left. \psi\left(\frac{3-\nu_e\tau_{cyc}}{4}\right)\right] \end{aligned} \tag{25}$$

Equation 24 shows that decoupling is not achieved by the periodic sequence of Figure 2a. Instead, the spin-locked magnetization is modulated by an averaged scalar coupling $\bar{J}$ given by eq 23 or by eq 19 when eq 17 is satisfied. Figure 3 shows $\bar{J}$, plotted as a function of $\nu_e\tau_{cyc}$, for different values of n. For large values of n, the maxima of $\bar{J}$ are strongly peaked for $\nu_e\tau_{cyc} = 2k+1$ as predicted by eq 18. $F_n(\nu_e\tau_{cyc})$ is a bound function, as shown in the inset of Figure 3; consequently, the cosinusoidal modulation of the magnetization depends on the ratio J/ν_e. Numerical calculations shown in Figure 3 also demonstrate that the same qualitative results are obtained from eqs 15 and 16. Because $\bar{H}^{(0)}$ is scaled by $1/n$, $\bar{J}$ or $F_n(\nu_e\tau_{cyc})$ obtained by integration of eq 16 and of eq 15 converge to one another for increasing values of n. The departure of eq 24 from a purely exponential decay introduces systematic errors into values of $R_{1\rho}$ measured experimentally, as described by Korzhnev et al.[23]

The form of eq 24 immediately suggests improved decoupling strategies. By fixing $n = 1$ and varying $\tau_{cyc} = \tau$, rather than fixing τ_{cyc} and varying n such that $n\tau_{cyc} = \tau$, the argument of the cosine function in eq 24 is bounded. Provided that the ratio J/ν_e is sufficiently small, eq 24 will be nearly exponential. This approach is embodied in Scheme 2 of Figure 1. Figure 4 compares $S'_z(t)$ plotted as a function of time for experiments

(40) Abramowitz, M.; Stegun, I. A. *Handbook of mathematical functions with formulas, graphs, and mathematical tables*; Dover Publications: New York, 1974.

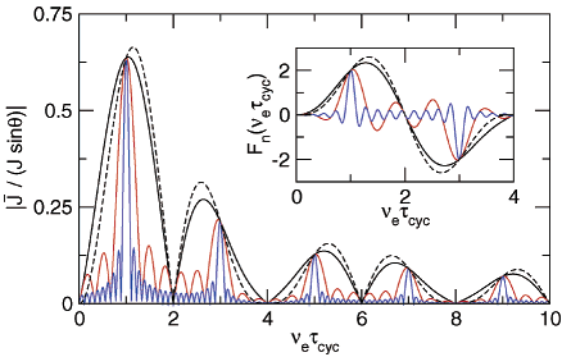

Figure 3. Incomplete decoupling by repetitive ^{1}H pulses. $|\bar{J}/J \sin\theta|$ is plotted against $\nu_e\tau_{cyc}$ for different values of n ($n = 1$ black, $n = 3$ red, and $n = 9$ blue); $2n$ is the number of ^{1}H π pulses applied during the ^{15}N spin-lock period $\tau = n\tau_{cyc}$, separated by a delay equal to $\tau_{cyc}/2$. The dashed line represents $|\bar{J}/J \sin\theta|$, for $n = 1$, obtained from the average Hamiltonian calculated by integrating all terms in eq 15. The inset shows $F_n(\nu_e\tau_{cyc})$, defined in eq 25, plotted against $\nu_e\tau_{cyc}$ for different values of n (the same legend applies). $F_n(\nu_e\tau_{cyc})$ is periodic with a period equal to 4 $\nu_e\tau_{cyc}$. The dashed line represents $F_n(\nu_e\tau_{cyc})$, for $n = 1$, obtained from the average Hamiltonian calculated by integrating all terms in eq 15.

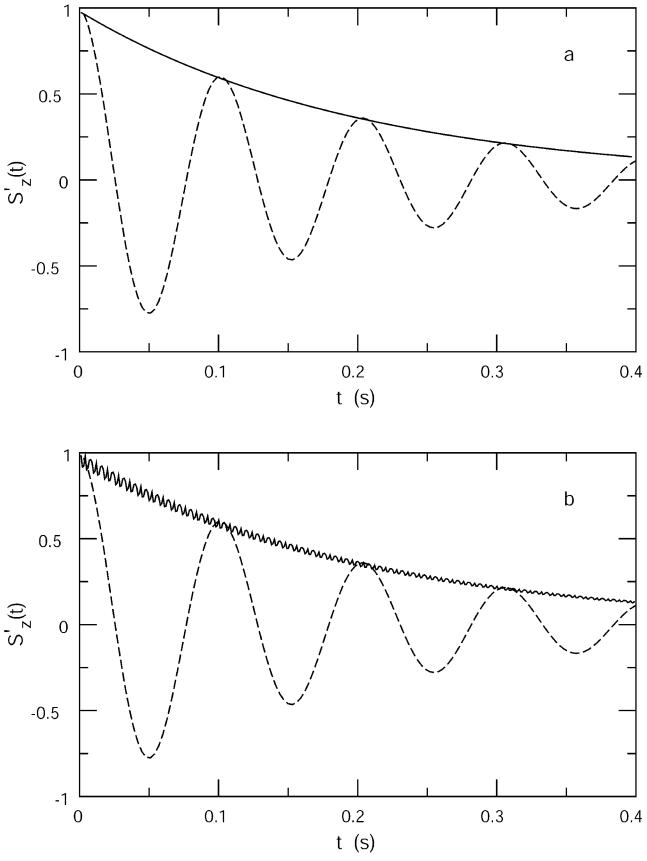

Figure 4. Time evolution of $S_z'(t)$ from eq 24 during the application of an on-resonance spin-lock field of strength equal to (a) 1000 Hz, and (b) 500 Hz. $S_z'(t)$ is modulated by an averaged scalar coupling $\bar{J}$ given by eq 23 with $n = 1$ (solid line) or by eq 19, when eq 17 is satisfied, with fixed $\tau_{cyc} = 3/\nu_e$ and variable n (dashed line).

that vary n and that vary τ_{cyc}. In accordance with theoretical expectations, cosinusoidal modulation of the decay is nearly absent when $n = 1$ and $\nu_e > 500$ Hz for $J = 92$ Hz.

A second conclusion drawn from the theoretical analysis is that any sequence of 180° ^{1}H decoupling pulses has a Fourier

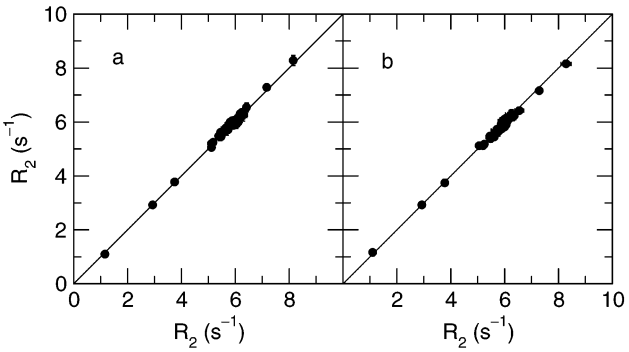

Figure 5. Comparison of R_2 values obtained using the three-pulse sequences presented in Figure 1. R_2 values obtained from Scheme 3 at a spin-lock field strength of 1018 ± 8 Hz are plotted on the x-axis in both panel a and b; the accuracy of the results have been established by Korzhnev and co-workers.[23] R_2 values obtained from Scheme 1 and from Scheme 2 are plotted on the y-axis of panel a and b, respectively. The spin-lock field strengths used were 1010 ± 7 Hz for Scheme 1 and 1022 ± 10 Hz for Scheme 2.

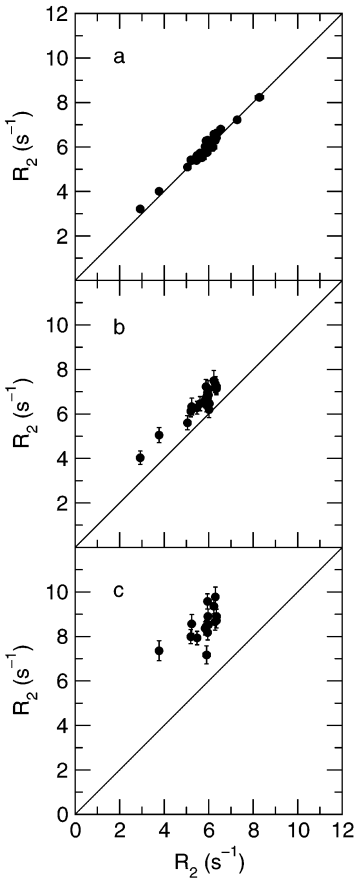

Figure 6. Comparison of R_2 values obtained from the pulse sequence depicted in Scheme 3 of Figure 1 at different spin-lock fields. The values of R_2 obtained with a spin-lock field strength equal to 1018 ± 8 Hz are plotted on the x-axis versus those obtained at 506 ± 6 Hz (a), 249 ± 3 Hz (b), and 156 ± 5 Hz (c) on the y-axis.

decomposition (although different from eq 4) and hence will generate a nonvanishing scalar coupling average Hamiltonian in the tilted reference frame. The pulse sequence shown as Scheme 1 in Figure 1 is designed to interupt the periodicity of the decoupling pulses by applying dephasing gradients while magnetization is stored along the z-axis of the laboratory reference frame.

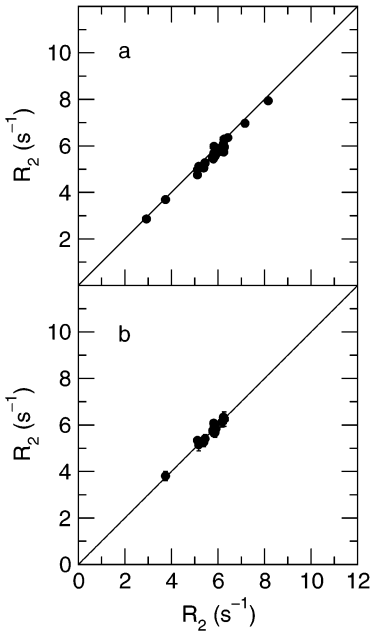

Figure 7. Comparison of R_2 values obtained from the pulse sequence presented in Scheme 2 of Figure 1 at different spin-lock fields. The values of R_2 obtained with a spin-lock field strength equal to 1022 ± 10 Hz are plotted on the *x*-axis versus those obtained at 506 ± 6 Hz (a) and 257 ± 6 Hz (b), on the *y*-axis.

As the ratio J/ν_e is reduced, higher order contributions to the average Hamiltonian are expected to become more important. The relative contribution of $\bar{H}^{(1)}$ to the average Hamiltonian is scaled by the ratio of the J/ν_e; the contributions of higher order terms $\bar{H}^{(p)}$ are expected to decrease as $(J/\nu_e)^p$.

4. Results

4.1. Comparison of the Different $R_{1\rho}$ Pulse Sequences. The three decoupling schemes presented in Figure 1 have been tested using the ubiquitin sample. Measured values of $R_{1\rho}$ for residues with $|\beta| < 0.4$ were converted to R_2 using eq 1 and measured values of R_1. Use of R_2, rather than $R_{1\rho}$, facilitates comparison between results recorded for different rf field strengths because R_2 does not depend on the tilt angle, which varies with field strength for any given resonance. The pulse sequence shown in Scheme 3 of Figure 1 has been proven to give accurate values of $R_{1\rho}$ and R_2 when the effective field $\nu_e \geq 1000$ Hz.[23] The values of $R_{1\rho}$ measured for ubiquitin using this sequence are the reference values for comparison with the other schemes in Figure 1.

Figure 5 shows that the new pulse sequences, Schemes 1 and 2 of Figure 1, yield accurate measurements of the $R_{1\rho}$ rate constants when ν_e is equal to 1000 Hz. Figure 6 shows that as ν_e is reduced below 250 Hz, the values of $R_{1\rho}$ measured with Scheme 3 become systematically overestimated. Figure 7 shows that the pulse sequence employing Scheme 2 gives accurate results for $R_{1\rho}$ for ν_e as low as 250 Hz. The magnetization decay profiles cannot be fit with single-exponential functions when $\nu_e = 150$ Hz (vide infra). Figure 8 shows that the pulse sequence depicted in Scheme 1 gives accurate values of $R_{1\rho}$ for field strengths as low as $\nu_e = 150$ Hz. Figure 9 shows the relaxation decay curves for residue Arg 72 of ubiquitin obtained for the three experiments using two spin-lock field strengths. When $\nu_e = 1000$ Hz, all three decoupling schemes yield magnetization decay profiles that are monoexponential. These results are

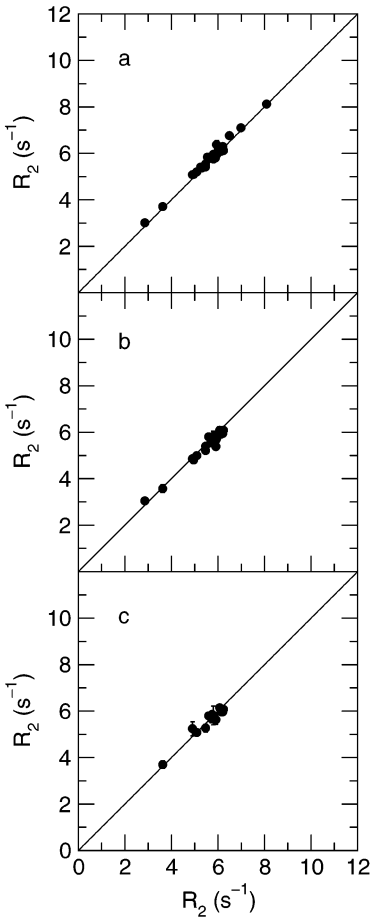

Figure 8. Comparison of R_2 values obtained from the pulse sequence depicted Scheme 1 of Figure 1 at different spin-lock fields. The values of R_2 obtained with a spin-lock field strength equal to 1010 ± 7 Hz are plotted on the *x*-axis versus those obtained at 508 ± 5 Hz (a), 249 ± 5 Hz (b), and 156 ± 5 Hz (c), on the *y*-axis.

consistent with the earlier experimental work of Korzhnev and co-workers[23] and with the theoretical analysis for Scheme 2 presented in eq 24 for $J/\nu_e \ll 1$. If $\nu_e = 150$ Hz, then the pulse sequence depicted in Scheme 3 shows three different decay regimes, each corresponding to a different number of ^{1}H 180° pulses applied during the spin-lock period, highlighted in different colors. As described above, because the decoupling scheme changes discontinuously each time another ^{1}H 180° pulse is added, a different average Hamiltonian is active during the different time periods of the experiment. The data shown for Scheme 2 exhibits an oscillatory behavior superimposed on the exponential decay. At this effective field strength, $J/\nu_e = 0.6$ and the modulation of the decay due to the function $F(\nu_e\tau_{cyc})$ in eq 24 is significant. Only Scheme 1 generates a monoexponential decay when $\nu_e = 150$ Hz. At even lower fields, where $J/\nu_e \approx 1$, even data recorded with Scheme 1 begins to show evidence of oscillatory behavior (not shown).

4.2. BPTI Dispersion Curve. Figure 10 shows the relaxation dispersion curve for residue Cys 14 of BPTI. Both on-resonance and off-resonance $R_{1\rho}$ experiments have been used to characterize dispersion over a wide range of ω_e. The on-resonance $R_{1\rho}$ experiment used the pulse sequence presented in Scheme 1 in Figure 1. The off-resonance $R_{1\rho}$ experiment uses the pulse sequence depicted in Scheme 2 of Figure 1 where the two ^{15}N 90° pulses preceding and following the spin-lock period have

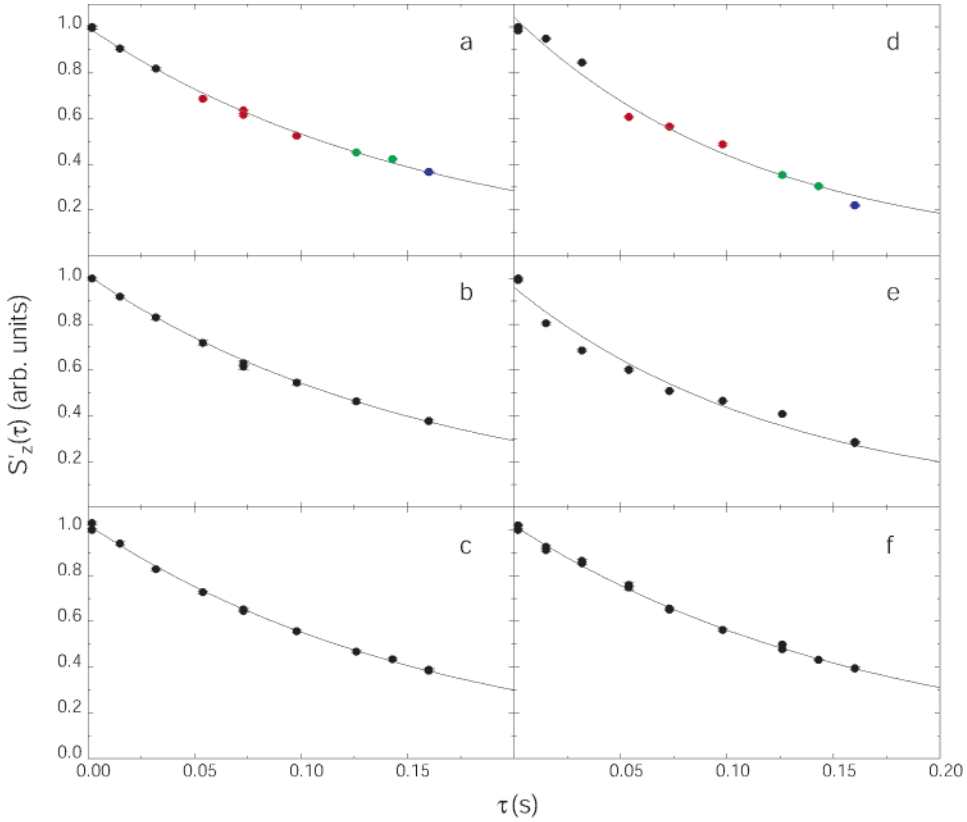

Figure 9. Relaxation decay curves for residue Arg 72, $\Omega = 11$ Hz, at two spin-lock field strengths, (a, b, c) 1010 Hz and (d, e, f) 150 Hz, for the experiments employing the pulse sequences presented in Figure 1, (a, d) Scheme 3, (b, e) Scheme 2, and (c, f) Scheme 1. In (a, d), the number of ^{1}H 180° pulses applied are (black) zero, (red) one, (green) two, and (blue) three.

been substituted by adiabatic pulses.[33] Data were fit using eqs 1 and 2 assuming fast exchange. A value of 6.09 ± 0.08 s^{-1} was used for R_2^0, measured as previously described.[41] Good agreement is apparent between the results of the off- and on-resonance $R_{1\rho}$ experiments in Figure 10. The results obtained from fitting of k_{ex} and Φ_{ex}, respectively, are equal to 7600 ± 200 s^{-1} and $28\,800 \pm 800$ s^{-2}. This value of k_{ex} is in agreement with a value of $\sim$7000 s^{-1} measured by CPMG experiments.[3] Using a value of $\delta\omega = 1360 \pm 90$ s^{-1}, obtained from a global analysis of CPMG dispersion data at three temperatures and two static magnetic field strengths,[3] we estimated $p_B = 1.6 \pm 0.2\%$ from Φ_{ex}, which agrees with a value of $1.3 \pm 0.2\%$ reported in the same study.[3]

Importantly, as Figure 10 highlights, the present results sample the relaxation dispersion curve at values of the effective rf field that are larger than those accessible by CPMG experiments. On the other hand, the values of $\nu_e \geq 1000$ Hz accessible in conventional on- and off-resonance $R_{1\rho}$ experiments alone are too strong to completely characterize the dispersion curve. Hence, the proposed pulse sequences (Schemes 1 and 2 in Figure 1) permit more complete characterization of the dispersion profile than either CPMG or conventional on- and off-resonance $R_{1\rho}$ experiments.

5. Discussion and Conclusion

In agreement with the local field approach,[23] the theoretical analysis of the $R_{1\rho}$ experiment suggests that incomplete decoupling results from periodic application of ^{1}H 180° pulses during the spin-lock period. The present analysis emphasizes that incomplete decoupling occurs because harmonic frequency components of the time-dependent J coupling, $a(t)$, are nearly matched to the effective frequency ω_e. Insights garnered from the theoretical treatment have been used to design two new pulse sequences aimed at providing accurate measurements of $R_{1\rho}$ for rf field strenths $<$1000 Hz. These experiments allow measurement of $R_{1\rho}$ relaxation rate constants for effective field strengths as low as 250 Hz for Scheme 2 and 150 Hz for Scheme 1 for ^{15}N spins in proteins with an ^{1}H$-^{15}$N scalar coupling constant of 92 Hz. The performance of the proposed experiments has been validated experimentally using both ubiquitin and BPTI. Similar experiments can be applied to rotating-frame relaxation of ^{1}H and ^{13}C spins.

The new techniques are accurate for a spectral region of $\pm 0.4\omega_1$ because placement of the magnetization along the direction of the effective field is necessary for accuracy of the $R_{1\rho}$ measurements. As the rf field strength decreases, a smaller region in the NMR spectrum is accessible to the $R_{1\rho}$ experiment. Thus, more than one $R_{1\rho}$ experiment with different spin-lock carrier offsets might be needed to measure the relaxation rate for all the spins of interest. For off-resonance $R_{1\rho}$ experiments with $\nu_e > 1000$ Hz, adiabatic sweeps are more effective that pulse-interupted free precession methods for aligning magnetization along the effective field.[33] In the present case, maintaining the adiabatic condition for weak rf fields results in very long adiabatic sweeps and relaxation losses become prohibitive.

(41) Wang, C.; Grey, M. J.; Palmer, A. G. *J. Biomol. NMR* **2001**, *21*, 361−366.

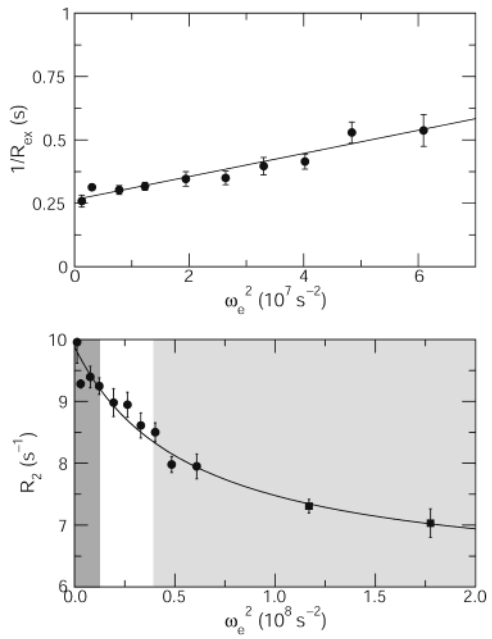

Figure 10. Relaxation dispersion for residue C14 of BPTI. The top panel shows $1/R_{ex}$ as a function of ω_e^2, calculated from the on-resonance $R_{1\rho}$ experiment using 10 field strengths ranging from 150 Hz and 1.2 kHz. The straight line shows the fit for fast exchange limit, with $k_{ex} = 7600 \pm 200$ s^{-1} and $\Phi_{ex} = 28\,800 \pm 800$ s^{-2}. In the bottom panel, R_2 is plotted against ω_e^2, the two points corresponding to the highest values of ω_e, represented as squares, have been obtained using the off-resonance $R_{1\rho}$ experiment as described in the text. The curve is drawn using the same values of k_{ex} and Φ_{ex} fitted from the data shown in the top panel. A value of 6.09 ± 0.08 s^{-1} was used for R_2^0 measured as previously described.[41] The dark and light gray areas of the plot represent the range of effective fields respectively accessible to CPMG ($\tau_{cyc} \geq 1$ms) and conventional on- and off-resonance $R_{1\rho}$ ($\nu_1 = \omega_1/2\pi \geq 1000$ Hz) experiments.

The new sequences suppress the contributions from $^{15}N-^{1}H$ dipole−dipole/^{15}N CSA relaxation by applying ^{1}H 180° pulses at $\tau/4$ and $3\tau/4$. This sequence element is sufficient to average relaxation interference to zero to second order in time.[21] A single pulse applied at $\tau/2$ would reduce the magnitude of $\bar{J}$ by a factor of 2 compared with the proposed experiments; however, a single pulse only averages the relaxation interference contribution to first order in time.[21] For this reason, we prefer the approach presented in Schemes 1 and 2 of Figure 1 for [*U*-^{15}N] proteins. In the case of [*U*-^{15}N; *U*-^{2}H] proteins, the difference between ^{15}N in-phase and anti-phase relaxation rate constants is smaller and a single 180° pulse may be sufficient to obtain good suppression of relaxation interference.[21]

When the applied rf field is very weak, scalar relaxation of the second kind[42] may contribute to the observed relaxation dispersion. As described in the Appendix, the relaxation rate constant for scalar relaxation in the rotating frame is given by

$$R_{1\rho}^{sc} = \begin{cases} R_{1H}\pi^2 J^2/(\omega_1^2 + \pi^2 J^2) & \omega_1 \geq \pi J, \\ R_{1H}\omega_1^2/(\omega_1^2 + \pi^2 J^2) & \omega_1 < \pi J \end{cases} \qquad (26)$$

in which R_{1H} is the longitudinal relaxation rate constant of the amide ^{1}H spin and the rf carrier is assumed to be positioned on-resonance with an average frequency of the two doublet components and $2\pi J \gg R_{1H}$. Although no evidence for this relaxation mechanism was observed in the present applications, reduction of the R_{1H} relaxation rate constant by deuteration of remote proton sites may be advisable in larger proteins.

CPMG and $R_{1\rho}$ rotating-frame relaxation experiments have been the choice for studying exchange processes that occur in the time scale range of microseconds to milliseconds.[2] CPMG sequences are sensitive to exchange processes with time constants in the range of hundreds of microseconds to milliseconds. $R_{1\rho}$ sequences can use much higher effective field strengths and for this reason have been used most often to characterize faster processes with smaller time constants, of the order of microseconds, that are inaccessible to CPMG experiments.

The proposed pulse sequences allow the use of lower effective fields and the characterization of slower processes that could not be studied until now by $R_{1\rho}$ relaxation dispersion. The possibility of employing both experimental methods to study exchange processes under the same experimental conditions allows an easier combination of the results obtained with these two techniques, giving access to an extended sampling of motional time scales.[10] Furthermore, to use new expressions for $R_{1\rho}$ outside the fast exchange limit recently presented by Palmer and co-workers,[15−17] low spin-lock field strengths must be utilized. The $R_{1\rho}$ experiment allows complete characterization of the kinetics of the exchange process using data acquired at a single static magnetic field strength, in contrast with the CPMG experiment that requires data at multiple magnetic field strengths. Most importantly, for systems outside the fast exchange limit, both magnitude and the sign of the chemical shift difference $\delta\omega$ of the exchanging species can be obtained from $R_{1\rho}$ experiments.[15] In contrast, CPMG experiments only measure the magnitude of $\delta\omega$, and additional experiments are required to determine the sign.[43−44] Knowledge of $\delta\omega$ is essential to gain insights into structural changes associated with exchange processes.[3]

An ever increasing number of applications of CPMG and $R_{1\rho}$ techniques to biological macromolecules are being reported. The new experiments presented herein promise to enlarge the range of biological dynamical phenomena that can be investigated by NMR spectroscopy.

Acknowledgment. This work was supported by National Institutes of Health Grants T32 HL07382 (E.J.), DK07328 (C.W.), GM40089 (M.R.), and GM59273 (A.G.P.). We thank Clay Bracken (Weill Medical College of Cornell University) for providing the ^{15}N sample of ubiquitin, and Dennis A. Torchia (National Institutes of Health) for helpful discussions.

Appendix

The evolution of an ^{15}N scalar-coupled doublet subject to scalar relaxation of the second kind, resulting from relaxation of the ^{1}H spin, is described by[42]

$$\frac{d}{dt}\begin{bmatrix} \boldsymbol{S}^{\alpha}(t) \\ \boldsymbol{S}^{\beta}(t) \end{bmatrix} = \begin{bmatrix} \boldsymbol{L}_{\alpha} - \boldsymbol{k} & \boldsymbol{k} \\ \boldsymbol{k} & \boldsymbol{L}_{\beta} - \boldsymbol{k} \end{bmatrix} \begin{bmatrix} \boldsymbol{S}^{\alpha}(t) \\ \boldsymbol{S}^{\beta}(t) \end{bmatrix} \qquad (A1)$$

in which

(42) London, R. E. *J. Magn. Reson.* **1990**, *86*, 410−415.
(43) Skrynnikov, N. S.; Dahlquist, F. W.; Kay, L. E. *J. Am. Chem. Soc.* **2002**, *124*, 12352−12360.
(44) Shaka, A. J.; Barker, P. B.; Freeman, R. *J. Magn. Reson.* **1985**, *64*, 547−552.

$$\boldsymbol{S}^{\alpha}(t) = \begin{bmatrix} S_x I^{\alpha}(t) \\ S_y I^{\alpha}(t) \\ S_z I^{\alpha}(t) \end{bmatrix} \tag{A2}$$

$$\boldsymbol{S}^{\beta}(t) = \begin{bmatrix} S_x I^{\beta}(t) \\ S_y I^{\beta}(t) \\ S_z I^{\beta}(t) \end{bmatrix} \tag{A3}$$

$$\boldsymbol{L}_{\alpha} = \begin{bmatrix} -R_2 & \Omega + \pi J & 0 \\ -\Omega - \pi J & -R_2 & \omega_1 \\ 0 & -\omega_1 & -R_1 \end{bmatrix} \tag{A4}$$

$$\boldsymbol{L}_{\beta} = \begin{bmatrix} -R_2 & \Omega - \pi J & 0 \\ -\Omega + \pi J & -R_2 & \omega_1 \\ 0 & -\omega_1 & -R_1 \end{bmatrix} \tag{A5}$$

$$\boldsymbol{k} = R_{1H}/2 \begin{bmatrix} 1 & 0 & 0 \\ 0 & 1 & 0 \\ 0 & 0 & 1 \end{bmatrix} \tag{A6}$$

and R_{1H} is the longitudinal relaxation rate constant for the ^{1}H spin. For simplicity, the rf carrier is assumed to be on-resonance with the Larmor frequency of the S spin; therefore $\Omega = 0$. In addition, the limit $\pi J \gg R_{1H}$ is assumed because resolved doublets normally are observable in protein NMR spectra. The rotating frame relaxation rate constant is given by

$$R_{1\rho} = R_2 + R_{1H}/2 - \lambda \tag{A7}$$

in which λ is a real eigenvalue of the matrix:

$$\begin{bmatrix} 0 & \pi J & 0 & R_{1H}/2 & 0 & 0 \\ -\pi J & 0 & \omega_1 & 0 & R_{1H}/2 & 0 \\ 0 & -\omega_1 & \Delta R & 0 & 0 & R_{1H}/2 \\ R_{1H}/2 & 0 & 0 & 0 & -\pi J & 0 \\ 0 & R_{1H}/2 & 0 & \pi J & 0 & \omega_1 \\ 0 & 0 & R_{1H}/2 & 0 & -\omega_1 & \Delta R \end{bmatrix} \tag{A8}$$

in which $\Delta R = R_2 - R_1$. The eigenvalues of this matrix are approximated by expanding the characteristic polynomial, truncating terms of order λ^3 or greater, and solving the resulting quadratic equation.[15] Two eigenvalues are obtained, corresponding to the case $\pi J < \omega_1$ and $\pi J \geq \omega_1$. Using the two approximate eigenvalues yields the final expressions:

$$R_{1\rho} = \begin{cases} \dfrac{\pi^2 J^2}{\pi^2 J^2 + \omega_1^2} R_1 + \dfrac{\omega_1^2}{\pi^2 J^2 + \omega_1^2} R_2 + R_{1H} \dfrac{\omega_1^2}{\pi^2 J^2 + \omega_1^2} & \pi J \geq \omega_1 \\ \dfrac{\pi^2 J^2}{\pi^2 J^2 + \omega_1^2} R_1 + \dfrac{\omega_1^2}{\pi^2 J^2 + \omega_1^2} R_2 + R_{1H} \dfrac{\pi^2 J^2}{\pi^2 J^2 + \omega_1^2} & \pi J < \omega_1 \end{cases} \tag{A9}$$

The terms proportional to R_1 and R_2 simply reflect the projection into tilted frames for each of the doublet components. The third term, proportional to R_{1H}, is the contribution to relaxation from scalar relaxation of the second kind in the presence of an on-resonance rf field and is identical to eq 26.

JA038721W